

# Journal of Geophysical Research: Solid Earth

## RESEARCH ARTICLE

10.1002/2017JB014340

### Special Section:

Earth and Space Science is  
Essential for Society

#### Key Points:

- Seismic velocity changes are highly correlated with areal strains due to volcano deformation
- The seismic velocity changes of about 1 or 2% occur at the depth of less than about 1 km at the volcano
- Estimated stress sensitivity of velocity changes shows depth dependent characteristics from comparing with the results reported in previous studies

#### Correspondence to:

T. Takano,  
takano@zisin.gp.tohoku.ac.jp

#### Citation:

Takano, T., T. Nishimura, and H. Nakahara (2017), Seismic velocity changes concentrated at the shallow structure as inferred from correlation analyses of ambient noise during volcano deformation at Izu-Oshima, Japan, *J. Geophys. Res. Solid Earth*, 122, doi:10.1002/2017JB014340.

Received 17 APR 2017

Accepted 14 AUG 2017

Accepted article online 17 AUG 2017

## Seismic velocity changes concentrated at the shallow structure as inferred from correlation analyses of ambient noise during volcano deformation at Izu-Oshima, Japan

Tomoya Takano<sup>1</sup> , Takeshi Nishimura<sup>1</sup> , and Hisashi Nakahara<sup>1</sup> 

<sup>1</sup>Department of Geophysics, Graduate School of Science, Tohoku University, Sendai, Japan

**Abstract** We investigate the stress sensitivity of velocity changes at Izu-Oshima in Japan using seismic interferometry method. We calculate cross correlation functions (CCFs) of ambient noises recorded by four seismic stations on the active volcano from 1 January 2012 to 31 December 2015 at 0.5–1 Hz, 1–2 Hz, and 2–4 Hz. Applying moving time windows to calculate cross spectrum between daily CCFs and reference CCF, which is the average for the all observation period, we compute daily velocity changes. The obtained velocity changes vary from –1% to 3% with a dominant period of about 1 year. We calculate areal strains by using Global Navigation Satellite Systems data at the volcano. It is evident that the velocity changes are well correlated with the areal strain changes whose linear trend is removed. The stress sensitivity of velocity changes, which are obtained from the observed velocity changes and areal strains, is lower at 0.5–1 Hz than that at higher frequencies:  $(7.1 \pm 1.3) \times 10^{-8} \text{ Pa}^{-1}$  at 0.5–1 Hz,  $(1.4 \pm 0.1) \times 10^{-7} \text{ Pa}^{-1}$  at 1–2 Hz, and  $(1.3 \pm 0.1) \times 10^{-7} \text{ Pa}^{-1}$  at 2–4 Hz. Modeling the velocity changes of Rayleigh wave propagating in layered structures, we find that the observed velocity changes are concentrated in the upper 1 km of the structure. Since similar frequency dependency is recognized among the stress sensitivity of velocity changes reported in previous studies, we conclude that the velocity changes are localized in the shallow depth because of the increase of confining pressure.

## 1. Introduction

Seismic velocity changes caused by large earthquakes or volcanic activities have been studied to understand the mechanical properties of the shallow structure. Such seismic velocity changes are measured by repeating earthquakes [Poupinet *et al.*, 1984] or active seismic sources [Nishimura *et al.*, 2005], but it is not easy to continuously monitor the properties of shallow structures because these seismic sources are sparse in time. It has been demonstrated that cross correlation function (CCF) of ambient noise converges to a Green's function between two receivers [Snieder, 2004]. The seismic velocity changes are then measured by comparing CCFs of ambient noise continuously obtained at a same seismic station pair. As a result, the noise correlation analyses succeeded in detecting seismic velocity changes due to large earthquakes in subduction zones [e.g. Nakata and Snieder, 2012; Minato *et al.*, 2012] or inland earthquakes [e.g. Brenguier *et al.*, 2008a; Takagi *et al.*, 2012; Hobiger *et al.*, 2012], inflation of volcanic edifice before eruption [Brenguier *et al.*, 2008b; Nagaoka *et al.*, 2010; Sens-Schönfelder *et al.*, 2014] or topographic change caused by an eruption [Anggono *et al.*, 2012], and seasonal variations such as precipitation [e.g. Sens-Schönfelder and Wegler, 2006].

The mechanisms of seismic velocity changes, which are still under investigations, are considered to originate mainly from the following three sources [e.g. Wegler *et al.*, 2009]. The first source is the strong ground motion that damages near-surface materials [e.g., Rubinstein and Beroza, 2004]. The seismic velocity reductions due to subsurface nonlinear behaviors caused by strong ground motion are observed at depths shallower than hundreds of meters, which is clarified from analyses of seismic data recorded at the top and bottom of a borehole [Sawazaki *et al.*, 2009; Takagi *et al.*, 2012; Nakata and Snieder, 2012]. The second source is the static stress (or strain) generated in the shallow structure due to a fault slip or volcanic activity [e.g., Brenguier *et al.*, 2008a]. Such seismic velocity changes are also observed in association with slow slip events at the plate boundary of Cocos plate, Mexico [Rivet *et al.*, 2011], volcanic activities [Ratdomopurbo and Poupinet, 1995; Hirose *et al.*, 2017], and the Earth tide [Takano *et al.*, 2014; Hillers *et al.*, 2015], which are not accompanied by strong ground motions. The third source is the seasonal changes generated by pore pressure changes

due to precipitation [Sens-Schönfelder and Wegler, 2006; Meier *et al.*, 2010] or variations of noise source distribution [Weaver *et al.*, 2009].

Among the above mentioned three mechanisms, the stress effect on the seismic velocity changes have been most quantitatively evaluated. For example, laboratory rock experiments have shown that the seismic velocities of rock increases with increasing confining pressure [Nur and Simmons, 1969]. Seismic analyses also have succeeded in evaluating the stress sensitivity of shallow structure or crust. *De Fazio et al.* [1973], *Reasenberg and Aki* [1974], *Yukutake et al.* [1988], and *Yamamura et al.* [2003] measured stress sensitivity of seismic velocity changes from temporal changes of travel times of *P* wave or Rayleigh wave due to the Earth tide using an artificial controlled source. The stress sensitivities of velocity changes are estimated to be from  $5 \times 10^{-7} \text{ Pa}^{-1}$  to  $2 \times 10^{-6} \text{ Pa}^{-1}$ . *Chen et al.* [2010] detected the seismic velocity changes of 0.02% due to the  $M_w$  7.9 Wenchuan earthquake using CCFs of ambient noise at the frequency of 0.33–1 Hz. The stress sensitivity of the velocity changes of  $0.5 \times 10^{-8} \text{ Pa}^{-1}$  is determined from the good agreement of spatial distributions between velocity changes and volumetric strain changes caused by the earthquake. *Nishimura et al.* [2005] measured seismic velocity changes caused by the  $M_6.1$  earthquake in 1998 and volcanic pressure sources at Iwate volcano in Japan using repeated active seismic experiments. They estimated the stress sensitivity of seismic velocity changes to be 0.3 to  $2 \times 10^{-7} \text{ Pa}^{-1}$  from the volumetric strain by the  $M_6.1$  fault and volcanic pressure sources. These previous studies clarified that seismic velocity changes in the shallow structure are surely dependent on the stress (or strain) changes, but the obtained stress sensitivities of seismic velocity changes vary from  $10^{-9} \text{ Pa}^{-1}$  to  $10^{-6} \text{ Pa}^{-1}$ .

This study aims to investigate the stress sensitivity of seismic velocity changes by analyzing ambient noise. Especially, we pay our attentions into the depth dependence of seismic velocity changes by analyzing ambient noises at different frequency bands. The target is Izu-Oshima, an active volcano in Japan. The volcano island is a proper field to investigate the stress sensitivity of the seismic velocity changes. This is because large earthquakes and eruptions are not observed at Izu-Oshima during the period we analyze ambient noise data so that strong ground motions or volcanic tremors do not contribute to observed seismic velocity changes. Also, seismic stations, GNSS stations, and rain gauge stations have been operated for more than 10 years at Izu-Oshima; thus, we can compare seismic velocity changes with strain changes or precipitation at the volcano. In the followings, we first calculate CCFs and examine their properties and estimate the seismic velocity changes. Subsequently, we compare the seismic velocity changes with areal strain changes to calculate the stress sensitivity of velocity changes. Finally, we discuss the depth dependency of the stress sensitivity of velocity changes.

## 2. Data

We analyze continuous seismic data and GNSS displacement data recorded at Izu-Oshima, whose activity is monitored by geophysical observations. Izu-Oshima is located at about 120 km to the south west of Tokyo, Japan, and the island rises approximately 1000 m from the seafloor, and its summit is 758 m high above the sea level. In recent years, moderate eruptions occurred in 1912, 1950, and 1986 which discharged several tens of million tons of volcanic material, and more than 20 small eruptions occurred from 1912 to 1986. After the volcanic activity from 1986 to 1987, long-period (more than 10 years) dilatational deformation is observed, being superimposed with short periodic (more than 1 year) deformation [Meteorological Research Institute (MRI), 2016]. Such periodic deformations are well correlated with volcanic earthquake activity and are explained by two volcanic pressure sources [MRI, 2016] (Figure 1). Since magnitudes of these earthquakes are less than about 3 [MRI, 2016], it is considered that strong motion does not cause damage in the shallow part of the volcanic edifice. The short periodic pressure source is located at depths of 3.7–5.1 km beneath the northern part of caldera formed in the central part of the island, and its volume change is estimated to be  $10^6 \text{ m}^3$  from 1 October 2009 to 30 April 2010. The other source generating the long periodic pressure change is located beneath the northern part of caldera at a depth of 6.7 km with volume changes of  $2.5 \times 10^7 \text{ m}^3$  from 2001 to 2010 [MRI, 2016].

We use continuous seismic data recorded at four stations of the Japan Meteorological Agency (JMA) network that are deployed on the volcano island (Figure 2). Distance between each seismic station ranges from about 3 to 10 km. A three component short period seismometer with a natural frequency of 1 Hz is installed at each station. V.OSFT, V.OSSN, and V.OSKT stations are equipped with a borehole type seismometer at depths of

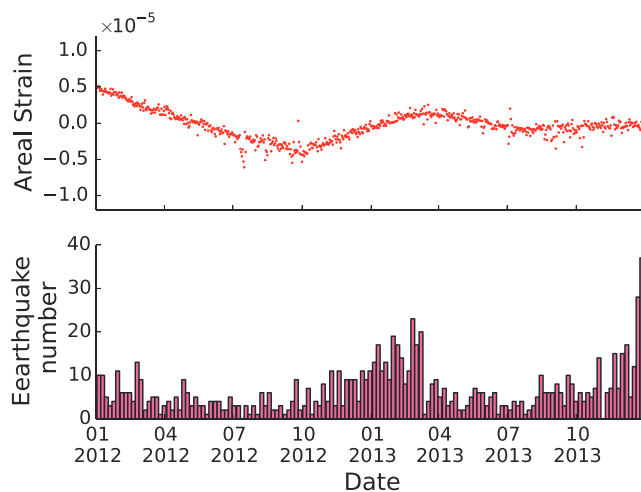


**Figure 1.** Volcanic activity at Izu-Oshima between 1 January 2012 and 31 December 2013. (top) Areal strain changes calculated by three GNSS stations on the volcano (see Figure 2). (bottom) Monthly number of volcanic earthquake.

92 m, 92 m, and 61 m, respectively, while V.OSMA station is equipped with a seismometer on the ground surface. Three of the four seismic stations are deployed at the northern part of the caldera, and V.OSFT station is located at the southern part of the caldera. The vertical components of short-period seismic data recorded from 1 January 2012 to 31 December 2015 are analyzed. These data are recorded with a sampling frequency of 100 Hz and an A/D resolution of 24 bit. We also use continuous coordinates data recorded at four stations of Geospatial Information Authority of Japan (GSI) network to estimate areal strain (Figure 2). The daily coordinates of the GNSS stations are distributed as “F3 solutions” [Nakagawa *et al.*, 2009].

### 3. Data Analyses

We calculate cross-correlation functions (CCFs) of ambient noises between six station pairs from the four seismic stations for 4 years from 2012 to 2015. We first cut the continuous seismic data at each station every 10 min, excluding the data containing earthquake signals and large unknown artificial noises, which are automatically detected by setting a threshold amplitude from the average root-mean-squared (RMS) amplitude. The continuous seismic data are filtered at 0.5–1 Hz, 1–2 Hz, and 2–4 Hz, and then one bit normalization is applied to enhance phase information [Bensen *et al.*, 2007]. The one bit ambient noise data at two stations are correlated every 10 min to obtain CCFs at the station pairs. Then, we obtain daily CCFs by stacking CCFs of  $\pm 10$  days to improve the signal to noise (S/N) ratio. We also calculate reference CCF at each station

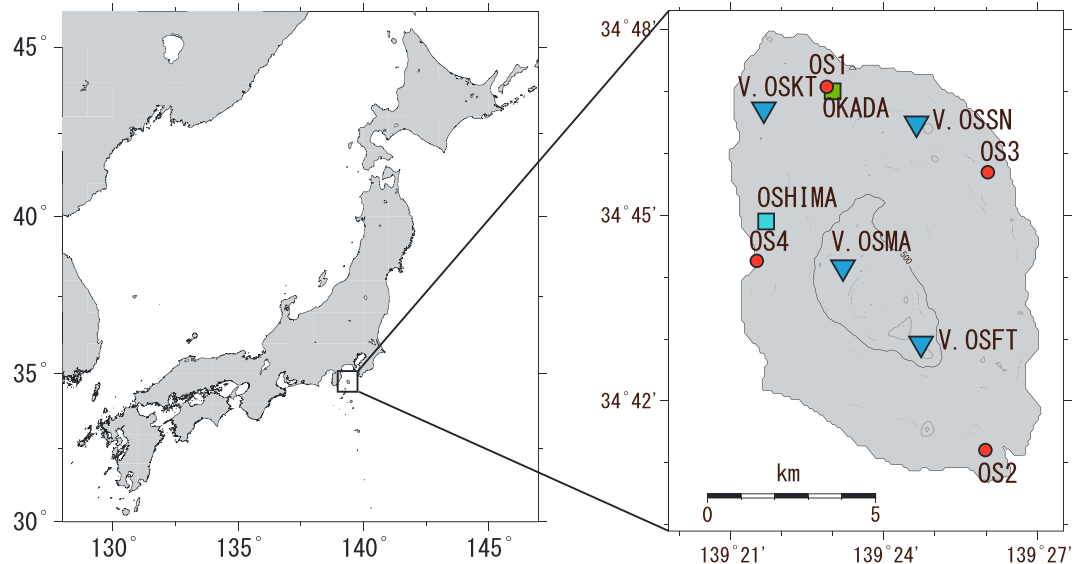


**Figure 2.** Locations of seismic, GNSS, and precipitation stations. (left) Location of Izu-Oshima volcano. (right) Enclosed area of the left figure with the locations of seismometers (blue inverted triangles). GNSS stations (red circles), a rain gauge (cyan square), and tidal gauge (green square).

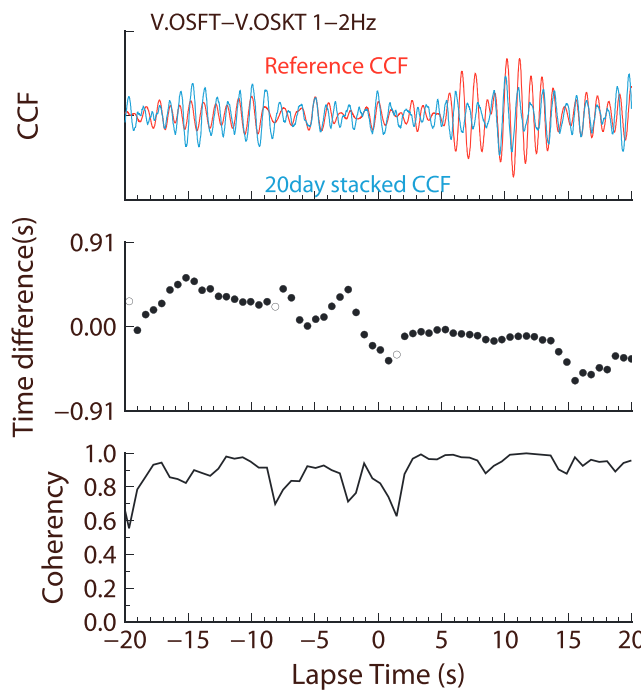


**Figure 3.** Example of the analyses of seismic velocity change. (top) a reference CCF (red line) and a daily CCF at 10 January 2012 (blue line) at the station pair of V.OSFT-V.OSSN. (middle) Time differences between daily and reference CCFs. Solid and open circles indicate time differences whose coherency are higher and lower than 0.7, respectively. (bottom) Coherency between the two CCFs.

to calculate seismic velocity changes (Figure 3). We also calculate seismic velocity changes at a wider frequency band of 1–4 Hz to test the stability of the MWCS measurements. The result show a similar tendency of seismic velocity changes as observed at the narrow frequency bands.

The reference CCFs between the station pair of V.OSFT and V.OSKT are shown in Figure 4. Wave packets with large amplitudes are seen at lapse times of about  $\pm 10$  s, although several large amplitudes are also found around  $\pm 4$  s at 2–4 Hz. As can be recognized in Figure 4, the amplitudes of CCFs in the positive lapse time are larger than those in the negative lapse time at 0.5–1 Hz throughout the whole period. The signals in the positive lapse time represent the waves propagating from V.OSFT to V.OSKT, which corresponds to almost from the east to the west. As noted by Stehly *et al.* [2006], when the noise sources are inhomogeneously distributed, energy flux between two stations indicates that the density of noise source is larger on one side than on the other at the station pairs. Biased amplitudes of CCFs in the negative and positive lapse times at the frequency band of 0.5–1 Hz and 1–2 Hz suggest that the noise sources are mainly distributed in the Pacific Ocean (Figure 5). On the other hand, at 2–4 Hz, wave packets with large amplitudes are seen in both the positive and negative lapse times. This implies homogeneous distribution of ambient noise sources and/or strong scattering properties of the shallow structure that can randomize wavefield even for nonisotropic noise distributions at higher frequency bands.

Figure 6 shows the record sections of CCFs at 0.5–1 Hz and 1–2 Hz. The wave packets with large amplitudes propagate with velocities of about 1 km/s for both of 0.5–1 Hz and 1–2 Hz. These propagation velocities are in agreement with the group velocities of Rayleigh wave that are predicted from the velocity structure at Izu-Oshima shown in Figure 7, which is obtained from the joint inversion of seismic data and gravity survey data [Onizawa *et al.*, 2002]. Since CCFs are extracted from the pairs of the vertical component of seismometers at a shallow depth less than 100 m, these large amplitudes are considered to be Rayleigh waves. On the other hand, such propagation of wave packets is not well recognized at 2–4 Hz. The reason is not clear, but ambient noises at 2–4 Hz may partly consist of scattered body waves as the seismic array analyses indicate [Bonnefoy-Claudet *et al.*, 2006; Koper *et al.*, 2010].

pair by stacking CCFs over the 4 years. Daily seismic velocity changes are measured by applying moving window cross spectrum (MWCS) method [Poupine *et al.*, 1984] between daily and the reference CCFs, in which phase differences ( $d\phi$ ) between a daily CCF and the reference CCF are related to the seismic velocity change ( $\frac{dv}{v}$ ) of structure:  $\frac{d\phi}{2\pi fT} = -\frac{dv}{v}$  where  $T$  is the lapse time,  $f$  is the dominant frequency, and  $v$  is the seismic velocity. The MWCS method can reduce the contamination of amplitude spectral changes on the seismic velocity changes because only phase spectra are used to estimate seismic velocity changes [Zhan *et al.*, 2013]. The phase differences are measured for the lapse times from  $-20$  s to  $+20$  s in which direct and coda waves propagating between the station pair are included. Analyzing long coda wave has a merit to avoid directivity effects generated from nonisotropic distributions of noise sources [Froment *et al.*, 2010]. Phase differences at the time windows with a coherency of more than 0.7 are used for fitting a regression line

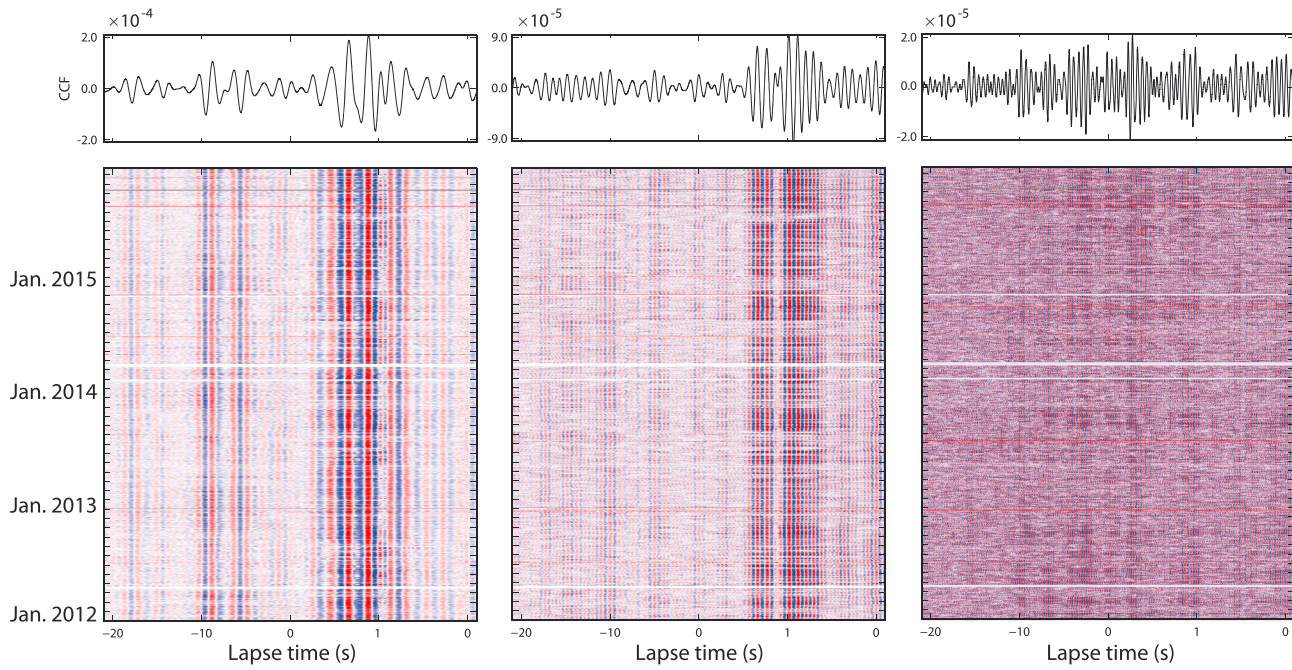


**Figure 4.** Examples of temporal variation of CCFs of station pair V.OSFT-V.OSKT at the three frequency bands: (left) 0.5–1.0 Hz, (middle) 1.0–2.0 Hz, (right) 2.0–4.0 Hz. Top panels represent the reference CCF at each frequency band. Red and blue color represent the amplitude of the daily CCFs: red color indicates positive, and blue color indicates negative. Color scale is normalized by maximum amplitude of reference CCF at each frequency band.

## 4. Results

### 4.1. Characteristics of Seismic Velocity Changes

Figure 8 shows daily seismic velocity changes calculated by comparing daily CCFs with the reference CCF for all seismic station pairs. It is apparent that seismic velocities at 1–2 Hz increase in August 2012, August 2013, and August 2015, while the seismic velocities decrease in April 2013, and from July 2014 to July 2015. Similar

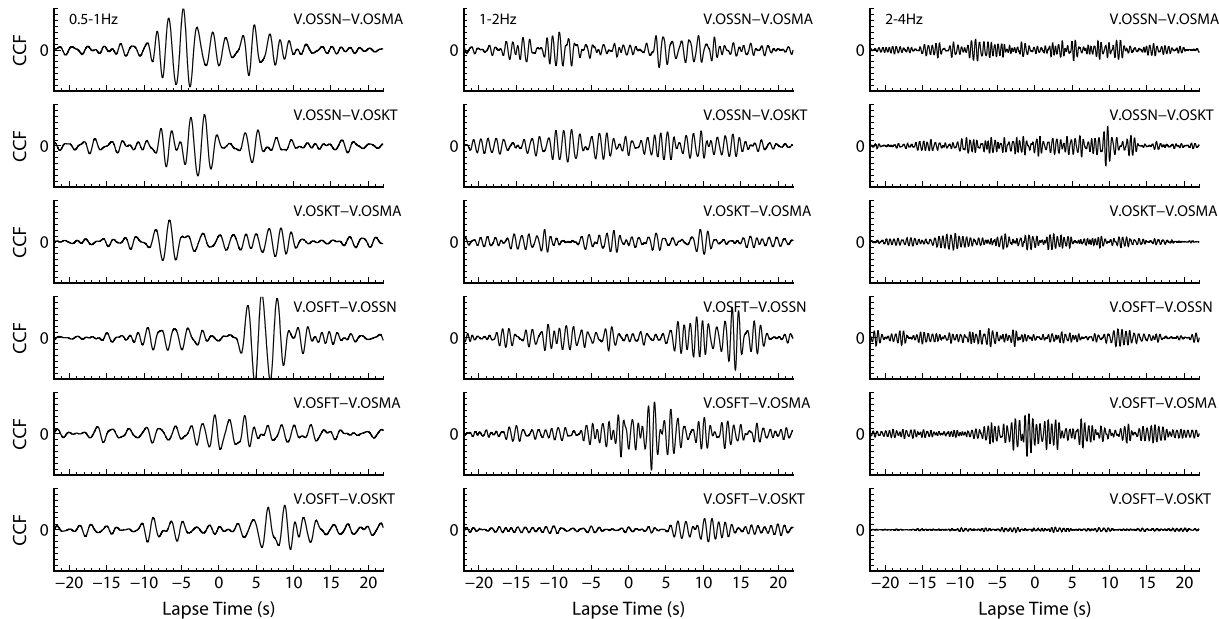


**Figure 5.** Reference CCFs at all station pair. Amplitude of CCFs are normalized by the maximum amplitude of each trace; (left) 0.5–1 Hz, (middle) 1–2 Hz, and (right) 2–4 Hz.

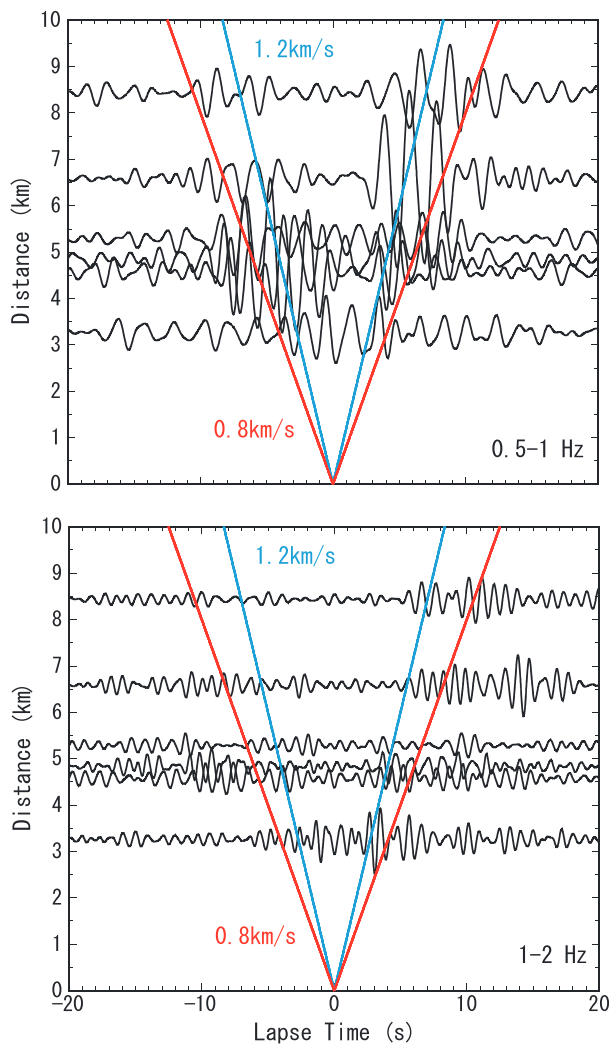


**Figure 6.** Record sections of CCFs at (top) 0.5–1 Hz and (bottom) 1–2 Hz. Red and blue lines indicate 0.8 km/s and 1.2 km/s propagation velocities, respectively.

displacements of the coordinate data at the four GNSS stations, each of which is an apex of a triangle with the latitude and longitude. We compute the average areal strain changes from the four triangles formed from the four GNSS stations with respect to the reference day of 1 January 2012. Figure 10 shows temporal changes of the averaged areal strain that are median filtered with a time window of 20 days, which is the same for the CCFs, to reduce the short-period noises. The observed areal strain changes shows yearly oscillations with an amplitude of about  $5 \times 10^{-6}$  strain.

We compare the seismic velocity changes with the areal strain changes and find that a linear trend of  $5 \times 10^{-6}$  strain/year is clearly recognized in the areal strain while not in the seismic velocity changes (see Figure 8). In the present study, we first remove the linear trend in the areal strain changes and compare it with the seismic velocity changes (Figure 10). It is well recognized that they are highly correlated with each other: the seismic velocity decreases during positive strain (dilatation) and increases during negative strain (contraction). Figure 11 displays the coherency and phase delays between the seismic velocity changes and areal strain changes after the removal of the linear trend. High coherency is recognized at the period of 1 year: the coherency averaged for all the station pairs are  $0.75 \pm 0.06$  at 0.5–1 Hz and  $0.73 \pm 0.06$  at 1–2 Hz, and  $0.76 \pm 0.07$  at 2–4 Hz, respectively. Also, no significant phase delay is observed between the seismic velocity change and areal strain changes at the period of more than 1 year.

temporal changes are found at the other frequency bands of all the six station pairs. The amplitudes of seismic velocity changes through the four years ranges from  $-1\%$  to  $3\%$  at 1–2 Hz for the six station pairs. The velocity changes at 0.5–1 Hz and 2–4 Hz are estimated to be  $-1\%$  to  $1\%$  and  $-1\%$  to  $2\%$ , respectively. The root-mean-squared (RMS) amplitude of seismic velocity changes averaged for all the six station pairs is  $(0.52 \pm 0.12)\%$  at 0.5–1 Hz,  $(0.76 \pm 0.17)\%$  at 1–2 Hz and  $(0.65 \pm 0.06)\%$  at 2–4 Hz, respectively. The RMS values of seismic velocity changes slightly increase with increasing the frequency. It is also recognized that the amplitudes of seismic velocity changes at V.OSSN-V.OSMA, which are located close to the summit area, are larger than those at the other station pairs especially around August in 2012 and January in 2015.

Figure 9 shows power spectra of the seismic velocity changes calculated at the three frequency bands. We find a peak at about 1 year for all the frequency bands.

#### 4.2. Comparison of Seismic Velocity Changes With Areal Strain Changes

To clarify the stress sensitivity of seismic velocity changes, we estimate the areal strain changes from the horizontal displacements of the four GNSS stations at Izu-Oshima (see Figure 2). We calculate the areal strain by using relative

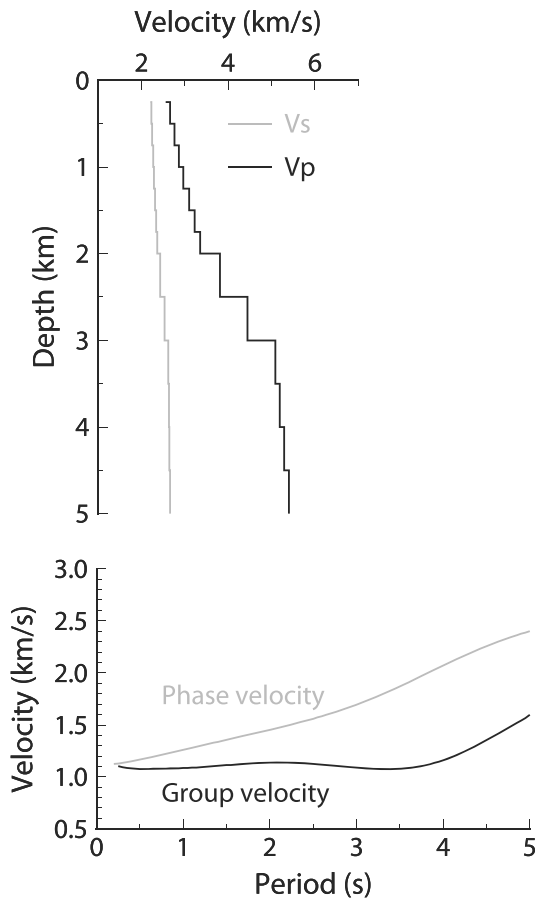


**Figure 7.** (top) Seismic velocity structure at Izu-Oshima by Onizawa *et al.* [2002]. Black line shows  $P$  wave velocity and gray line shows  $S$  wave velocity. (bottom) Dispersion curve of phase velocity (gray line) and group velocity (black line) derived by the velocity structure at Izu-Oshima.

and  $5.9 \times 10^{-8}$  at 2–4 Hz. These stress sensitivities are about one third of those estimated from areal strain without linear trend. The reason why a slope of linear trend of velocity changes is smaller than that of raw areal strain changes is unclear. It is necessary to accumulate the data and clarify their relationship at longer periods of a few years to understand the response mechanism of seismic velocity changes to the areal strain changes.

#### 4.3. Comparison of Seismic Velocity Changes With Precipitation

Since Sens-Schönfelder and Wegler [2006] pointed out that the seismic velocity changes at Merapi volcano are well correlated with ground water level changes by precipitation rather than volcanic activities, we examine the effect of precipitation on the seismic velocity changes at Izu-Oshima. In general, the seismic velocity changes due to precipitation are interpreted as pore pressure changes at the shallow part of structure that are caused by water level changes [Wegler *et al.*, 2009]. First, the present study simply compares the daily precipitation data at a JMA station (OSHIMA in Figure 2) with the observed seismic velocity changes. As shown in Figure 12a, the seismic velocity changes do not reduce nor change when large amounts of precipitation are observed. To quantitatively evaluate their relations, we calculate coherency and phase delay between the precipitations and seismic velocity changes after removing offsets of the observed daily precipitations. The results show that coherencies are small for all the seismic station pairs. The average is  $0.06 \pm 0.09$  at 0.5–1 Hz,  $0.03 \pm 0.03$  at 1–2 Hz,  $0.14 \pm 0.19$  at 2–4 Hz at the dominant period (1 year) of the seismic velocity changes. To take into account the drainage of the ground water after rain, we further calculate coherencies between the seismic velocity changes and precipitation averaged for 90 days. The results

Strain sensitivity of the seismic velocity changes is calculated for each station pair by fitting a regression line between the seismic velocity changes and areal strain changes. The strain sensitivity of seismic velocity changes averaged for the six station pairs is estimated to be  $(1.3 \pm 0.2) \times 10^3$  at 0.5–1 Hz,  $(2.6 \pm 0.3) \times 10^3$  at 1–2 Hz, and  $(2.4 \pm 0.1) \times 10^3$  at 2–4 Hz. For the bulk modulus of 18 GPa, which is calculated from the seismic velocity structure at Izu-Oshima [Onizawa *et al.*, 2002], the stress sensitivity of seismic velocity changes is estimated to be  $(7.1 \pm 1.3) \times 10^{-8} \text{ Pa}^{-1}$  at 0.5–1 Hz,  $(1.4 \pm 0.1) \times 10^{-7} \text{ Pa}^{-1}$  at 1–2 Hz, and  $(1.3 \pm 0.1) \times 10^{-7} \text{ Pa}^{-1}$  at 2–4 Hz. Smaller stress sensitivity is observed at 0.5–1 Hz.

We also give attention to the linear trend. The seismic velocities seem to slightly increase with time. For the period from 1 July 2014 to 1 May 2015 when large fluctuations are not observed, the seismic velocities at 0.5–1 Hz, 1–2 Hz, and 2–4 Hz increase 0.4%, 0.7%, and 1.1%, respectively. Comparing these with the linear trend of the areal strain changes, we estimate the stress sensitivity of velocity changes averaged for all station pairs to be  $2.4 \times 10^{-8}$  at 0.5–1 Hz,  $4.1 \times 10^{-8}$  at 1–2 Hz,

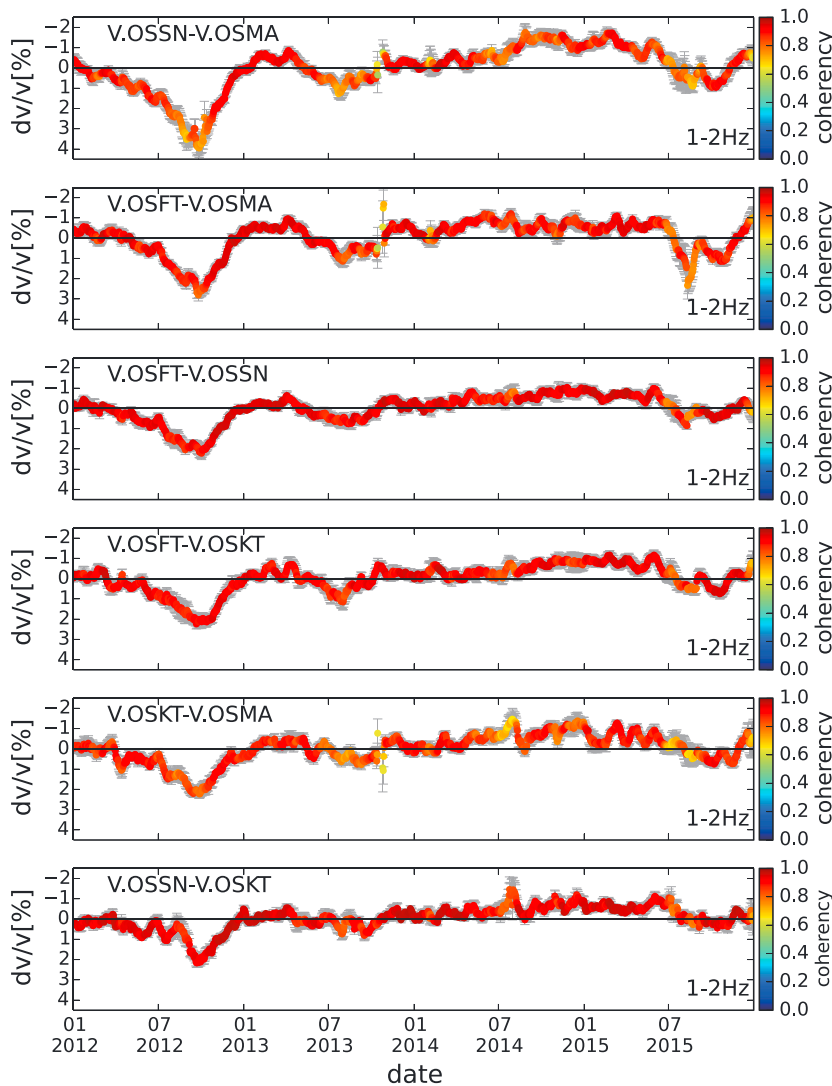


**Figure 8.** Seismic velocity changes with error bar from 1 January 2012 to 31 December 2015 are shown. The results at the frequency band of 1–2 Hz are shown. A color scale is coherency between a reference and a daily CCF.

also indicate small coherencies for all the seismic station pairs (Figure 12b). We thus conclude that there is no significant correlation between the seismic velocity changes and precipitation at Izu-Oshima. However, we also find that the coherencies between velocity changes and precipitation at the period of about 30 day is more than 0.4, which indicates precipitation may be one of the candidate for the short-term fluctuations in seismic velocity.

#### 4.4. Comparison of Seismic Velocity Changes With Sea Level

An oceanic loading may contribute to the strain changes in the crust or the shallow structure of Izu-Oshima because the volcano is a small island surrounded by the Pacific ocean. The oceanic loading bends the land, and sea level rise makes the land dilative. Averaged daily sea heights observed by a tide gauge at a JMA station (OKADA, Figure 2) show seasonal variations with a peak-to-peak height of about 50 cm (Figure 13), which overburdens 5 Pa on the ocean bottom. We use the sea height data for 3 years from January 2012 to December 2014 during which the data is available from JMA website. As indicated in Figure 13, the seismic velocity changes and sea height changes look weakly correlated, as their coherency indicates more than 0.5 at periods of more than 1 year. To assess the effect of sea height on the seismic velocity changes, we compare the observed and predicted areal strains induced by the oceanic loading. For the sake of simplicity, we

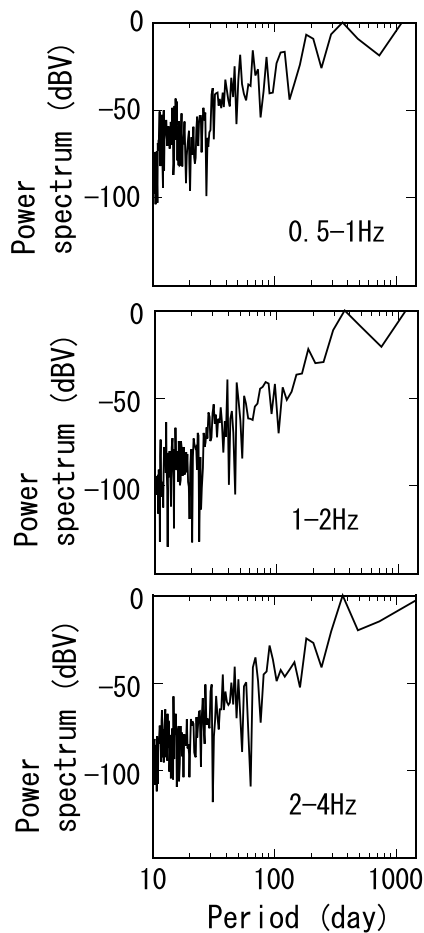


**Figure 9.** Power spectrum of seismic velocity changes at (left) 0.5–1 Hz, (middle) 1–2 Hz, and 2–4 Hz (right) at station pair of V.OSFT-V.OSSN.

assume that the island is represented as a circle shape with a radius of 4.5 km, which is the width of island in the east-west direction, and the oceanic loading of 5 Pa, which corresponds to  $\pm 50$  cm sea height change, work on the ocean bottom from the coast to 20 km from the center of island. Then, we calculate line strain  $\varepsilon_r$  based on Boussinesq's problem [Farrell, 1972]

$$\varepsilon_r = \frac{20\text{km}^2 \pi r_H (1 - 2\nu)p}{2G(r + r_H)^2} \text{d}r \text{d}\theta \quad (1)$$

where  $r_H$  is the radius of the land,  $p$  the loading pressure,  $\nu$  Poisson's ratio, and  $G$  rigidity of the medium. The line strain is estimated to be  $1.4 \times 10^{-7}$  at a center point of the island. This is one order lower than the observed areal strains by GNSS. Therefore, we conclude that the oceanic loading is not a main cause of the long-term seismic velocity changes measured at Izu-Oshima. It is recognized that seismic velocity increase during the high sea height (e.g., in the autumn of 2012). However, since high-sea height generates dilatation in the volcanic edifice, the observed correlation is inconsistent with the interpretation based on opening/closing of pores due to stress changes.

## 5. Discussion

### 5.1. Spatial Distribution of Seismic Velocity Changes and Areal Strain Changes

We documented in section 4.1 that the seismic velocity changes are almost same among all the station pairs (Figure 8). On the other hand, we notice that the amplitude of velocity changes at the pairs of V.OSSN-V.OSMA and V.OSMA-V.OSFT, which are the pairs of the stations located closely to the active central summit, are slightly larger than the other pairs. Especially, large differences of temporal changes are recognized for the period from August to October 2012. To understand such spatial distributions of the seismic velocity changes, we examine the areal strain changes at August 2012, when large areal strains are observed. We apply a spherical pressure source in the semiinfinite medium [Mogi, 1958] to the observed displacements at the four GNSS stations in August 2012. The pressure source is determined at a depth of 6.7 km beneath the summit caldera ( $34.724^\circ\text{N}$ ,  $139.403^\circ\text{E}$ ) with a volume change of  $-2.7 \times 10^6 \text{ m}^3$ , which is located at almost the same location ( $34.74^\circ\text{N}$ ,  $139.4^\circ\text{E}$ ) determined by JMA.

The location errors of our study are about 1 km and 3 km in the horizontal and vertical directions, respectively.

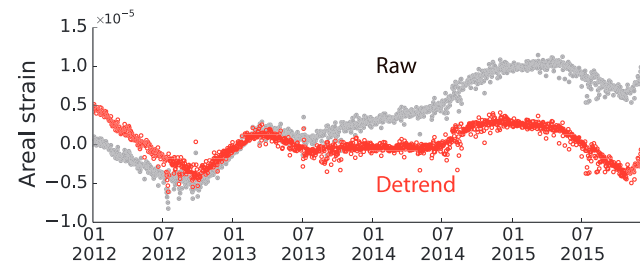


**Figure 10.** Temporal changes of the areal strain at Izu-Oshima from January 2012 to December 2015. (gray dots) Raw areal strain. (red open circles) The areal strain after removing a linear trend.

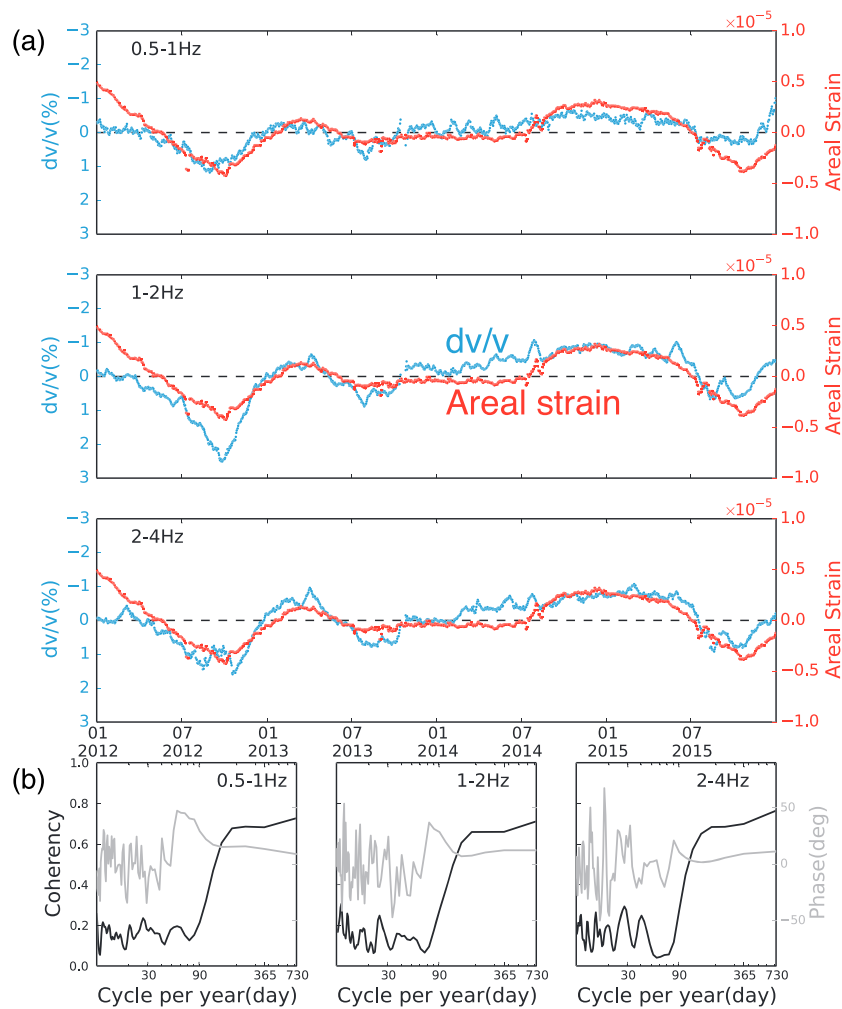


**Figure 11.** (a) Comparison of the seismic velocity changes averaged for all station pairs with the detrended areal strain: (top) 0.5–1 Hz, (middle) 1–2 Hz, and (bottom) 2–4 Hz. Blue dots are seismic velocity changes and red dots are areal strain changes. (b) Coherency (black line) and phase delay (gray line) calculated by cross spectrum between seismic velocity changes and areal strain; (left) 0.5–1 Hz, (center) 1–2 Hz, (right) 2–4 Hz.

Based on the estimated spherical pressure source, we calculate spatial distribution of the areal strain (Figure 14). Large areal strains are observed at the summit area where V.OSSN and V.OSFT are located. Also, large seismic velocity changes tend to be observed at the station pairs whose seismic ray paths cross the summit area (i.e., the seismic station pairs of V.OSSN-V.OSMA, V.OSSN-V.OSFT, and V.OSFT-V.OSMA). The seismic velocity changes estimated from coda parts of CCFs have high sensitivity around the stations, as the sensitivity kernels of coda wave to seismic velocity changes shows two peaks both at the source and receiver locations [Pacheco and Snieder, 2006]. These considerations suggest that the observed seismic velocity changes are mainly caused by the stress changes of the volcanic pressure source.

We mention that the seismic velocity changes are slightly deviated from the areal strain changes for some observation periods: for example, from September to October in 2012 and from August to December in 2015 (Figure 11). Such inconsistency may represent an existence of other sources that cause the seismic velocity changes. Izu-Oshima is an active volcano so that contribution of gas or fluid injection from a deeper part of the volcano may change the medium property, since the laboratory experimental data indicate the  $P$  and  $S$  waves changes due to existence of gas or fluid in pores of rocks [Ito et al., 1979]. However, we do not have volcanic gas observation data and the volcanic earthquake activity was not high at these periods (Figure 1). Hence, we are not able to clarify the origins now.

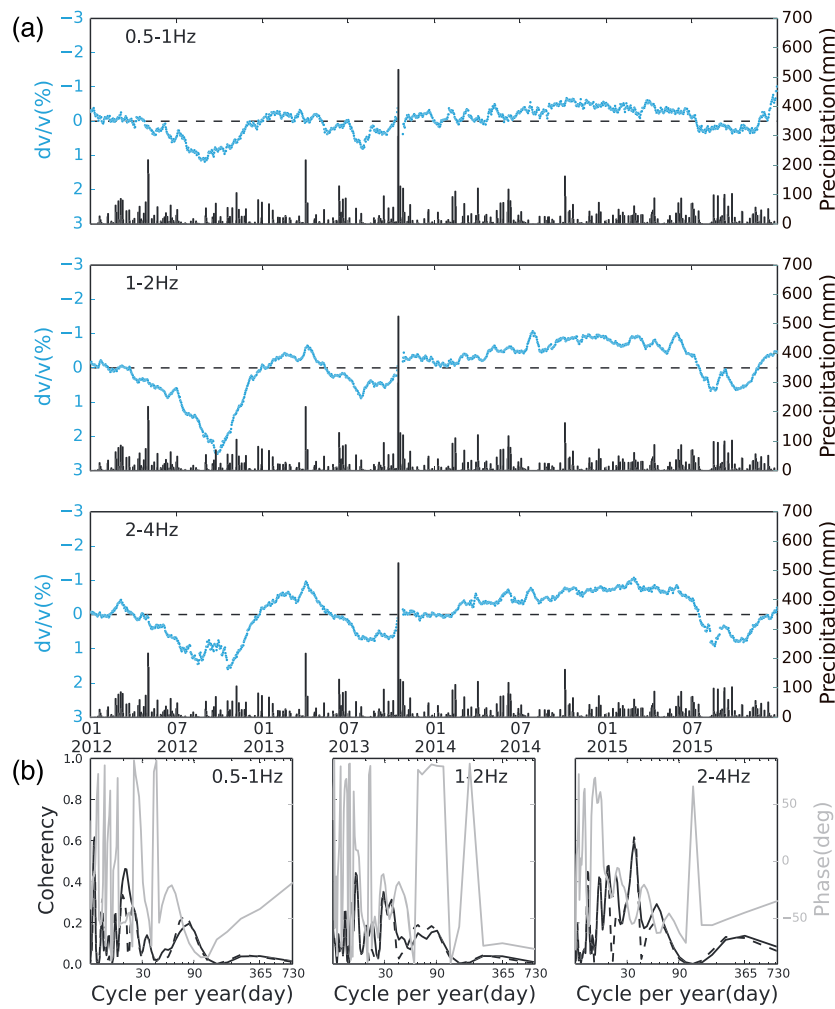


**Figure 12.** (a) Comparison between the seismic velocity changes averaged for all station pairs and rainfall. (top) 0.5–1 Hz, (middle) 1–2 Hz, (bottom) 2–4 Hz. Blue dots are the seismic velocity changes and black bars are daily rainfalls. (b) Coherency and phase delay between seismic velocity changes averaged for all station pairs and 1 day precipitation (black lines), coherency between seismic velocity changes and precipitation averaged by moving window of 90 days (black dashed lines); (left) 0.5–1 Hz, (center) 1–2 Hz, and (right) 2–4 Hz.

## 5.2. Stress Sensitivity of Seismic Velocity Changes at Different Depths

We have demonstrated that the seismic velocity changes at 0.5–1 Hz show lower values than those at the higher-frequency ranges. We explain such frequency dependent characteristics by considering a depth-dependent stress sensitivity of seismic velocity changes.

Since the main phases in the CCFs are considered to be Rayleigh waves, we calculate theoretical stress sensitivity at the three frequency bands as follows. First, phase velocities of Rayleigh wave are calculated based on the *P* and *S* wave velocity structure by *Onizawa et al.* [2002] (see Figure 7). The density,  $\rho$ , is estimated from an empirical relationship of  $\rho = 0.31 \times V_p^{0.25}$  [*Gardner et al.*, 1974], where  $V_p$  is the *P* wave velocity (we call this structure model as “reference structure”). Second, we compute phase velocities of Rayleigh wave for a structure model in which seismic velocity at each layer is slightly changed from the reference structure. Then, we calculate the difference of phase velocity between the structure model and the reference structure. Finally, the theoretical stress sensitivity of the velocity changes is calculated by dividing the difference of phase velocity by the expected stress of  $9.0 \times 10^4$  Pa during the observation period, which is estimated from the maximum areal strain of  $5 \times 10^{-6}$  and a bulk modulus of 18 GPa.

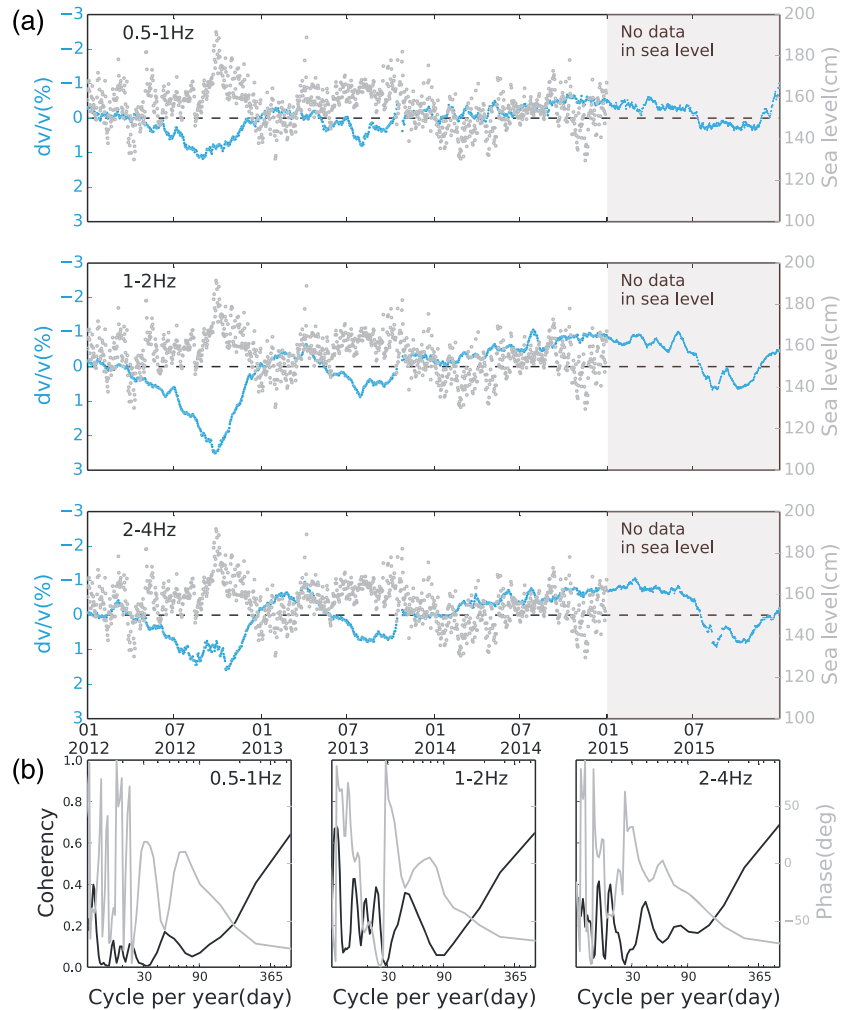


**Figure 13.** (a) Comparison between the seismic velocity changes averaged for all station pairs and sea height; (top) 0.5–1 Hz, (middle) 1–2 Hz, (bottom) 2–4 Hz. Blue dots are the seismic velocity changes and gray dots are sea level. (b) Coherency (black line) and phase delay (gray line) calculated by cross spectrum between seismic velocity changes and sea height; (left) 0.5–1 Hz, (center) 1–2 Hz, (right) 2–4 Hz.

We examine two structure models shown in Figure 15. Model 1 reduces seismic velocity with  $\chi$  % only at the upper layer with a thickness of  $H$  (top of Figure 16). Model 2 decreases the seismic velocity linearly with depth. The seismic velocity change is  $\chi$  % at the top and converges to zero at a depth of  $H$  (bottom of Figure 16). The following misfit function for the theoretical stress sensitivity  $S^{\text{cal}}$  and the observed one  $S^{\text{obs}}$  is used to search the best fit model:

$$\text{misfit} = \frac{1}{6} \sum_{i=1}^6 \{ S^{\text{obs}}(f_i) - S^{\text{cal}}(f_i) \}^2 \quad (2)$$

Here  $i$  represents the frequency band. Adding to the stress sensitivity at 0.5–1 Hz, 1–2 Hz, and 2–4 Hz that are estimated in the section 4.2, we use the stress sensitivities at 0.375–0.75 Hz, 0.75–1.5 Hz, and 1.5–3 Hz that are obtained from CCFs at those frequency ranges (open circles with a bar in Figure 15). We search the best fit model by changing the parameters  $\chi$  and  $H$  that minimize the misfit function for each model. Red lines in Figure 15 indicate the best fit models. Model 1 with  $H$  of 1.0 km and  $\chi$  of 1.0% and Model 2 with  $H$  of 1.0 km and  $\chi$  1.6% well explain the observation. We do not see any significant differences of the fitness between Models 1 and 2, but both models indicate that the seismic velocity changes with about 1 or 2% occur at the shallow depth of less than about 1 km. Note that the contamination of body waves to

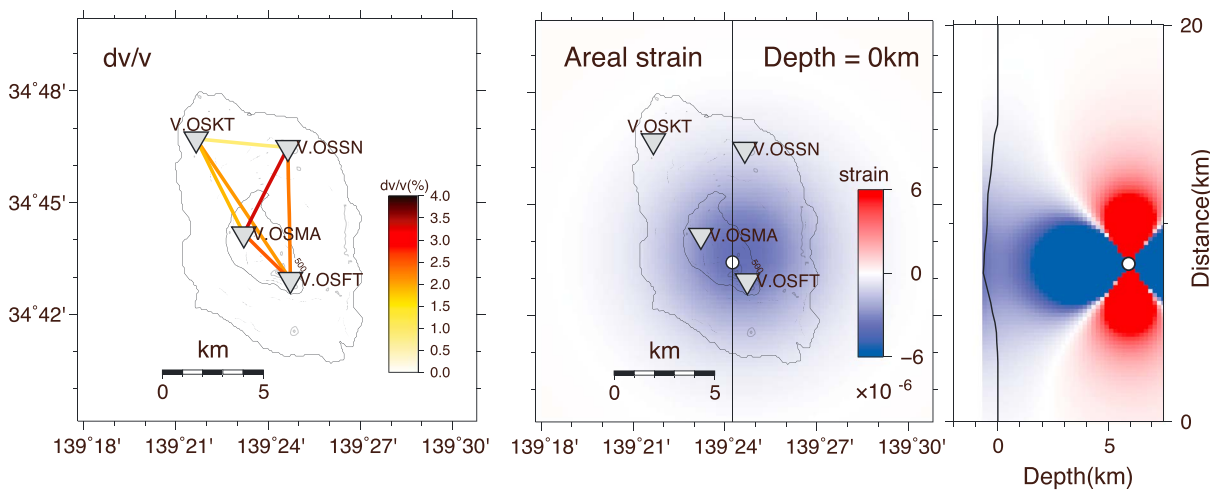


**Figure 14.** (a) Seismic velocity changes estimated from daily CCFs on 21 August in 2012. (b) The areal strain estimated from a spherical pressure source model is shown. (c) Vertical cross section of the areal strain along black line shown in Figure 14b. Blue color indicates contraction, red color indicates dilatation. White circle indicates the pressure source.

ambient noises may affect the depth sensitivity of velocity changes, especially at the high frequency band of 2–4 Hz. However, the estimated parameters  $\chi$  and  $H$  are mostly determined by the lower frequency band data.

The stresses are estimated to be  $1.5 \times 10^4$  Pa at the subsurface and  $1.2 \times 10^4$  Pa at a depth of 1 km above the volcanic pressure source of  $2.7 \times 10^6$  m<sup>3</sup> located at a depth of 6.7 km. These stresses are much smaller than

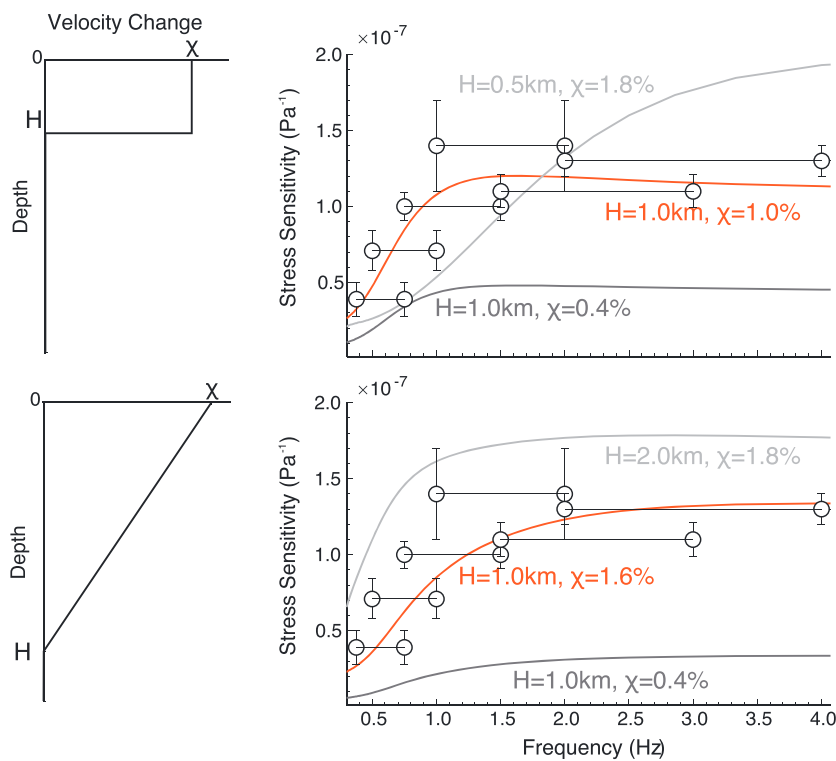


**Figure 15.** (left) The velocity change Models 1 (top) and 2 (bottom). (right) Comparison of the stress sensitivities estimated from the CCF analyses (open circles) and those predicted from the velocity change models (colored lines) for the parameters of depth  $H$  and velocity change  $\chi$ .

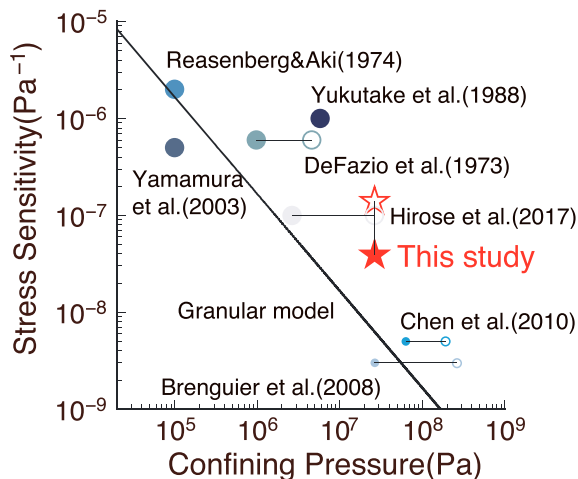


**Figure 16.** The stress sensitivity reported in the previous studies and the present study vs confining pressure (see detail in text). Stars are the stress sensitivity at Izu-Oshima estimated by the present study. Solid circles are the stress sensitivity determined at the other regions by previous studies. Black line represents the stress sensitivity predicated from the granular model. The data that may be affected by dynamic strain changes are plotted with smaller symbols.

the confining pressure of  $2.6 \times 10^7$  Pa at a depth of 1 km due to the lithostatic equilibrium. These estimations suggest that the confining pressure is a main cause that reduces the seismic velocity changes at the deeper part of structure. We further compare the stress sensitivity estimated at Izu-Oshima with the results reported at other regions. From the seismic velocity changes reported in Reasenberg and Aki [1974], De Fazio et al. [1973], Yukutake et al. [1988], and Yamamura et al. [2003] that use the Earth tide and active source, we estimate the stress sensitivity of seismic velocity changes to be  $5 \times 10^{-7}$  to  $2 \times 10^{-6}$  Pa<sup>-1</sup> from the theoretical tidal stress of  $10^3$  Pa. The depths where structures change are inferred to be about 0 to 200 m, because the seismic waves analyzed are more than 30 Hz and the source and receivers are located on the ground surface or in a

mine at shallow depths. Seismic velocity changes due to stress changes of Rayleigh wave that is extracted from CCFs of ambient noises. Here we estimate the stress sensitivity of velocity changes at a given depth by considering the one wavelength of Rayleigh waves. Hirose et al. [2017] detected the seismic velocity changes caused by the changes of magma pressure at Sakurajima volcano from ambient noise analyses at 1–8 Hz. We estimate the stress sensitivity of velocity changes to be  $1.0 \times 10^{-7}$  Pa<sup>-1</sup> at the depth of 0.1–1 km. Brenguier et al. [2008a] detected the seismic velocity changes related with the postseismic relaxation after the 2004 Parkfield earthquake ( $M_w$  6.0) from ambient noise analyses at 0.1–0.9 Hz. Since the postseismic stress change is calculated to be 0.2 MPa [Freed et al., 2007], we estimate the stress sensitivity of seismic velocity changes of  $3.0 \times 10^{-9}$  Pa<sup>-1</sup> at the depth of 1.1–10 km. Chen et al. [2010] analyzes ambient noises before and after the 2008 Wenchuan earthquake ( $M_w$  7.9) in China. Since the Rayleigh waves are at 0.33–1 Hz, we estimate the stress sensitivity to be  $0.5 \times 10^{-8}$  Pa<sup>-1</sup> at the depth of 0.2–3 km. Note that the strong ground motion may also introduce seismic velocity changes at subsurface at the same time. Hence, the results for the data from Brenguier et al. [2008a] and Chen et al. [2010] may contain the contribution from the dynamic strain changes. These stress sensitivity data are plotted in Figure 16 against the confining pressure that is computed from the depth by assuming lithostatic equilibrium. It is clearly recognized that the observed stress sensitivity of seismic velocity changes decreases with increasing confining pressure,  $p$ . It is noted that we calculate the wavelengths of Rayleigh wave by assuming the phase velocity of 1 km/s for simplicity. In addition, the depths may be overestimated because vertical displacement of Rayleigh wave decreases at the depth of about one fourth of wavelength [Aki and Richards, 2002]. Our estimations of the confining pressure may be overestimated or underestimated, but the tendency of the pressure dependent stress sensitivity does not change because wide frequency data are compared.

Pressure-dependent characteristics may be explained by a granular theory [Mindlin, 1949; Mavko et al., 2009]. In the granular theory, the medium including pores is modeled as packed dry identical spheres, and the effective elastic properties of the medium is expressed by a function of porosity, the average number of contacts per sphere, sphere radius, and normal and tangential stiffness between two spheres. The shear wave velocity  $V_s$  is derived by the effective shear modulus  $G_{eff}$  [Mavko et al., 2009]:

$$G_{eff} = \frac{5 - 4v}{5(2 - v)} \sqrt{\frac{3C^2(1 - \varphi)^2 G^2}{2\pi^2(1 - v)^2}} p \quad (3)$$

where  $\nu$  is the Poisson's ratio,  $G$  is shear modulus of the solid grains,  $C$  is the average number of contacts per sphere, and  $\phi$  is porosity. Therefore, a confining pressure dependence of seismic velocity changes can be expressed by differentiating with respect to pressure:

$$\frac{1}{V_s} \frac{\partial V_s}{\partial p} = \frac{1}{6p} \quad (4)$$

The predicted stress sensitivity fairly well explains the confining pressure dependence of the observed stress sensitivities (Figure 16). This consistency suggests that the seismic velocity changes in the shallow structure are caused by opening and closure of pores in the medium. The stress sensitivity based on the granular theory can be used for the estimation of stress sensitivity of seismic velocity changes at different depths.

## 6. Conclusion

We have examined the origins of seismic velocity changes associated with the edifice deformations due to volcanic activity at Izu-Oshima. The observed seismic velocity changes with periods of 1 year or less are well correlated with the areal strains caused by volcanic pressure sources at a depth of about 6 km rather than precipitations and oceanic loading, although long-term linear trend is not recognized in the seismic velocity changes but in the areal strains. The stress sensitivity of seismic velocity changes is estimated to be  $(7.1 \pm 1.3) \times 10^{-8}$  at 0.5–1 Hz,  $(1.4 \pm 0.1) \times 10^{-7}$  at 1–2 Hz, and  $(1.3 \pm 0.1) \times 10^{-7}$  at 2–4 Hz. The theoretical velocity changes of Rayleigh wave shows that the stress sensitivity of the seismic velocity changes decreases at the depth of more than 1 km in Izu-Oshima. Comparing the stress sensitivity of velocity changes at Izu-Oshima with the results reported in previous studies, we find a significant depth dependence of the stress sensitivity of the seismic velocity changes.

## Acknowledgments

We thank the Japan meteorological Agency for providing us with continuous seismic data which were downloaded from the Data Management Center of the National Research Institute for Earth Science and Disaster Resilience (<http://www.hinet.bosai.go.jp>), precipitation data (<http://www.data.jma.go.jp>), and sea height level data (<http://www.jodc.go.jp>) and Geospatial Information Authority of Japan for providing us with GNSS daily coordinates (<http://terras.gsi.go.jp>). Some of the figures were made using the Generic Mapping Tool (Wessel and Smith 1998). Thoughtful comments of Yosuke Aoki and two anonymous reviewers improved the manuscript. We thank Andre Revil for his editorial efforts. Tomoya Takano is grateful for support from the Japan Society for the Promotion of Science (JSPS) and the Ministry of Education, Culture, Sports, Science and Technology (MEXT) of Japan, under its Observation and Research Program for Prediction of Earthquakes and Volcanic Eruptions.

## References

- Aki, K., and P. G. Richard (2002), *Quantitative Seismology*, 2nd ed., Univ. Science Books, Sausalito, Calif.
- Angono, T., T. Nishimura, H. Sato, H. Ueda, and M. Ukawa (2012), Spatio-temporal changes in seismic velocity associated with the 2000 activity of Miyakejima volcano as inferred from cross-correlation analyses of ambient noise, *J. Volcanol. Geotherm. Res.*, 247–248, 93–107, doi:10.1016/j.volgeores.2012.08.001.
- Bensen, G. D., M. H. Ritzwoller, M. P. Barmin, A. L. Levshin, F. Lin, M. P. Moschetti, N. M. Shapiro, and Y. Yang (2007), Processing seismic ambient noise data to obtain reliable broad-band surface wave dispersion measurements, *Geophys. J. Int.*, 169, 1239–1260, doi:10.1111/j.1365-246X.2007.03374.x.
- Bonnefoy-Claudet, S., F. Cotton, and P. Y. Bard (2006), The nature of noise wavefield and its applications for site effects studies. A literature review, *Earth Sci. Rev.*, 79(3–4), 205–227, doi:10.1016/j.earscirev.2006.07.004.
- Brenguier, F., M. Campillo, C. Hadzioannou, N. M. Shapiro, R. M. Nadeau, and E. Larose (2008a), Postseismic relaxation along the San Andreas Fault at Parkfield from continuous seismological observation, *Science*, 321, 1478–1481, doi:10.1126/science.1160943.
- Brenguier, F., N. M. Shapiro, M. Campillo, V. Ferrazzini, Z. Duputel, O. Coutant, and A. Nercessian (2008b), Towards forecasting volcanic eruptions using seismic noise, *Nat. Geosci.*, 1, 126–130.
- Chen, J. J., B. Froment, Q. Y. Liu, and M. Campillo (2010), Distribution of seismic wave speed changes associated with the 12 May 2008 Mw 7.9 Wenchuan earthquake, *Geophys. Res. Lett.*, 37, L18302, doi:10.1029/2010GL044582.
- De Fazio, T. L., K. Aki, and J. Alba (1973), Solid earth tide and observed change in the in situ seismic velocity, *J. Geophys. Res.*, 78, 1319–1322.
- Farrell, W. E. (1972), Deformation of the Earth by surface loads, *Rev. Geophys.*, 10, 761–797, doi:10.1029/RG010i003p00761.
- Freed, A. M., S. T. Ali, and R. Bürgmann (2007), Evolution of stress in Southern California for the past 200 years from coseismic, postseismic and interseismic stress changes, *Geophys. J. Int.*, 169, 1164–1179, doi:10.1111/j.1365-246X.2007.03391.x.
- Froment, B., M. Campillo, P. Roux, P. Gouédard, A. Verdel, and R. Weaver (2010), Estimation of the effect of non-isotropically distributed energy on the apparent arrival time in correlations, *Geophysics*, 75(5), SA85–SA93, doi:10.1190/1.3483102.
- Gardner, G. H. F., L. W. Gardner, and A. R. Gregory (1974), Formation velocity and density—The diagnostic basics for stratigraphic traps, *Geophysics*, 39, 770–780, doi:10.1190/1.1440465.
- Hillers, G., L. Retailleau, M. Campillo, A. Inbal, J.-P. Ampuero, and T. Nishimura (2015), In situ observations of velocity changes in response to tidal deformation from analysis of the high-frequency ambient wavefield, *J. Geophys. Res. Solid Earth*, 120, 210–225, doi:10.1002/2014JB011318.
- Hirose, T., H. Nakahara, and T. Nishimura (2017), Combined use of repeated active shots and ambient noise to detect temporal changes in seismic velocity: Application to Sakurajima volcano, Japan, *Earth Planets Space*, 69, 42, doi:10.1186/s40623-017-0613-7.
- Hobiger, M., U. Wegler, K. Shiomi, and H. Nakahara (2012), Coseismic and postseismic elastic wave velocity variations caused by the 2008 Iwate-Miyagi Nairiku earthquake, Japan, *J. Geophys. Res.*, 117, B09313, doi:10.1029/2012JB009402.
- Ito, H., J. DeVille, and A. Nur (1979), Compressional and shear waves in saturated rock during water-steam transition, *J. Geophys. Res.*, 84, 4731–4735, doi:10.1029/JB084iB09p04731.
- Koper, K. D., K. Seats, and H. Benz (2010), On the composition of Earth's short-period seismic noise field, *Bull. Seismol. Soc. Am.*, 100(2), 606–617, doi:10.1785/0120090120.
- Mavko, G., T. Mukerji, and J. Dvorkin (2009), *The Rock Physics Handbook: Tools for Seismic Analysis in Porous Media*, 2nd ed., Cambridge Univ. Press, New York.
- Meier, U., N. M. Shapiro, and F. Brenguier (2010), Detecting seasonal variations in seismic velocities within Los Angeles basin from correlations of ambient seismic noise, *Geophys. J. Int.*, 181, 985–996, doi:10.1111/j.1365-246X.2010.04550.x.

- Minato, S., T. Tsuji, S. Ohmi, and T. Matsuoka (2012), Monitoring seismic velocity change caused by the 2011 Tohoku-oki earthquake using ambient noise records, *Geophys. Res. Lett.*, 39, L09309, doi:10.1029/2012GL051405.
- Mindlin, R. D. (1949), Compliance of elastic bodies in contact, *J. Appl. Mech.*, 16, 259–268.
- Mogi, K. (1958), Relations between the eruptions of various volcanoes and the deformations of the ground surfaces around them, *Bull. Earthquake Res. Inst.*, 36, 99–134, doi:10.1016/j.epsl.2004.04.016.
- Meteorological Research Institute (MRI) (2016), Crustal deformations around Izu-Oshima Volcano [in Japanese], *Rep. Coord. Comm. Predict. Volcanic Eruption*, 136, 17–25.
- Nagaoka, Y., K. Nishida, Y. Aoki, and M. Takeo (2010), Temporal change of phase velocity beneath Mt. Asama, Japan, inferred from coda wave interferometry, *Geophys. Res. Lett.*, 37, L22311, doi:10.1029/2010GL045289.
- Nakagawa, H., et al. (2009), Development and validation of GEONET new analysis strategy (version 4) [in Japanese], *J. Geogr. Surv. Inst.*, 118, 1–8.
- Nakata, N., and Snieder, R. (2012), Estimating near-surface shear wave velocities in Japan by applying seismic interferometry to KiK-net data, *J. Geophys. Res.* 117, B01308, doi:10.1029/2011JB008595.
- Nishimura, T., S. Tanaka, T. Yamawaki, H. Yamamoto, T. Sano, M. Sato, and H. Sato (2005), Temporal changes in seismic velocity of the crust around Iwate volcano, Japan, as inferred from analyses of repeated active seismic experiment data from 1998 to 2003, *Earth Planets Space*, 57(6), 491–505.
- Nur, A., and G. Simmons (1969), The effect of saturation on velocity in low porosity rocks, *Earth Planet. Sci. Lett.*, 7, 183–193.
- Onizawa, S., H. Mikada, H. Watanabe, and S. Sakashita (2002), A method for simultaneous velocity and density inversion and its application to exploration of subsurface structure beneath Izu-Oshima volcano, Japan, *Earth Planets Space*, 54, 803–817.
- Pacheco, C., and R. Snieder (2006), Time-lapse traveltime change of singly scattered acoustic waves, *Geophys. J. Int.*, 165(2), 485–500, doi:10.1111/j.1365-246X.2006.02856.x.
- Poupinet, G., W. L. Ellsworth, and J. Frechet (1984), Monitoring velocity variations in the crust using earthquake doublets: An application to the Calaveras fault, California, *J. Geophys. Res.*, 89, 5719–5731.
- Ratdomopurbo, A., and G. Poupinet (1995), Monitoring a temporal change of seismic velocity in a volcano: Application to the 1992 eruption of Mt. merapi (Indonesia), *Geophys. Res. Lett.*, 22, 775–778, doi:10.1029/95GL00302.
- Reasenberg, P., and K. Aki (1974), A precise, continuous measurement of seismic velocity for monitoring in situ stress, *J. Geophys. Res.*, 79, 399–406.
- Rivet, D., M. Campillo, N. M. Shapiro, V. Cruz-Atienza, M. Radiguet, N. Cotte, and V. Kostoglodov (2011), Seismic evidence of nonlinear crustal deformation during a large slow slip event in Mexico, *Geophys. Res. Lett.*, 38, L08308, doi:10.1029/2011GL047151.
- Rubinstein, J. L., and G. C. Beroza (2004), Evidence of widespread nonlinear strong ground motion in the  $M_w$  6.9 Loma Prieta earthquake, *Bull. Seismol. Soc. Am.*, 94, 595–1608.
- Sawazaki, K., H. Sato, H. Nakahara, and T. Nishimura (2009), Time-lapse changes of seismic velocity in the shallow ground caused by strong ground motion shock of the 2000 Western-Tottori Earthquake, Japan, as revealed from coda deconvolution analysis, *Bull. Seismol. Soc. Am.*, 99(1), 352–366, doi:10.1785/0120080058.
- Sens-Schönfelder, C., and U. Wegler (2006), Passive image interferometry and seasonal variations of seismic velocities at Merapi Volcano, Indonesia, *Geophys. Res. Lett.*, 33, L21302, doi:10.1029/2006GL027797.
- Sens-Schönfelder, C., E. Pomponi, and A. Peltier (2014), Dynamics of Piton de la Fournaise volcano observed by passive image interferometry with multiple references, *J. Volcanol. Geotherm. Res.*, 276, 32–45, doi:10.1016/j.jvolgeores.2014.02.012.
- Snieder, R. (2004), Extracting the Green's function from the correlation of coda waves: A derivation based on stationary phase, *Phys. Rev. E*, 69, 046610, doi:10.1103/physRevE.69.046610.
- Stehly, L., M. Campillo, and N. M. Shapiro (2006), A study of the seismic noise from its long-range correlation properties, *J. Geophys. Res.*, 111, B10306, doi:10.1029/2005JB004237.
- Takagi, R., T. Okada, H. Nakahara, N. Umino, and A. Hasegawa (2012), Coseismic velocity change in and around the focal region of the 2008-Iwate-Miyagi Nairiku earthquake, *J. Geophys. Res.*, 117, B06315, doi:10.1029/2012JB009252.
- Takano, T., T. Nishimura, H. Nakahara, Y. Ohta, and S. Tanaka (2014), Seismic velocity changes caused by the Earth tide: Ambient noise correlation analyses of small-array data, *Geophys. Res. Lett.*, 41, 6131–6136, doi:10.1002/2014GL060690.
- Weaver, R., B. Froment, and M. Campillo (2009), On the correlation of non-isotropically distributed ballistic scalar diffuse waves, *J. Acoust. Soc. Am.*, 126(4), 1817–1826, doi:10.1121/1.3203359.
- Wegler, U., H. Nakahara, C. Sens-Schönfelder, M. Korn, and K. Shiomi (2009), Sudden drop of seismic velocity after the 2004  $M_w$  6.6 mid-Niigata earthquake, Japan, observed with Passive Image Interferometry, *J. Geophys. Res.*, 114, B06305, doi:10.1029/2008JB005869.
- Yamamura, K., O. Sano, H. Utada, Y. Takei, S. Nakao, and Y. Fukao (2003), Long-term observation of in situ seismic velocity and attenuation, *J. Geophys. Res.*, 108(B6), 2317, doi:10.1029/2002JB002005.
- Yukutake, H., T. Nakajima, and K. Doi (1988), In situ measurements of elastic wave velocity in a mine, and the effects of water and stress on their variation, *Tectonophysics*, 149, 165–175.
- Zhan, Z., V. C. Tsai, and R. W. Clayton (2013), Spurious velocity changes caused by temporal variations in ambient noise frequency content, *Geophys. J. Int.*, 194(3), 1574–1581, doi:10.1093/gji/ggt170.